

## INVERSE-SQUARE LAW VIOLATION AND REACTOR ANTINEUTRINO ANOMALY

*D. V. Naumov\**, *V. A. Naumov\*\**, *D. S. Shkirmanov\*\*\**

Joint Institute for Nuclear Research, Dubna

We discuss a possibility that the so-called reactor antineutrino anomaly can be, at least in part, explained by applying a quantum field-theoretical approach to neutrino oscillations, which in particular predicts a small deviation from the classical inverse-square law at short but macroscopic distances between the neutrino source and detector. An extensive statistical analysis of the reactor data is performed to examine this speculation.

PACS: 13.15.+g; 25.30.Pt

### INTRODUCTION

Nuclear reactors are intense sources of electron antineutrinos whose spectrum is composed of thousands of spectral components formed mainly by the  $\beta$  decay of the fission products of the four parent isotopes:  $^{235}\text{U}$ ,  $^{238}\text{U}$ ,  $^{239}\text{Pu}$ , and  $^{241}\text{Pu}$ . The very sophisticated recent calculations [1–3] yield a net 3–3.5% upward shift in the predicted energy-averaged  $\bar{\nu}_e$  flux with respect to the previously expected flux used in the earlier short baseline (SBL) reactor experiments (ILL–Grenoble [4,5], Gösgen [6], Krasnoyarsk [7,8], Rovno [9–11], Bugey [12,13], Savannah River Plant [14]). The  $\bar{\nu}_e$  flux normalization uncertainty in the new calculations is claimed to be only  $\pm 2.7\%$ . This implies [3] that the measured event rates in the SBL experiments are about 6% too low, giving rise to the so-called “reactor antineutrino anomaly” (RAA).

Figure 1 illustrates this issue. The curve shows the ratio of the  $\bar{\nu}_e$ -induced event rate calculated with and without regard for the  $3\nu$  oscillations. Here and thereafter we use the global best fit values for the neutrino mass-squared splittings and mixing angles from [15] for the normal mass hierarchy; we also assume no  $CP$  violation in mixing. The cross section for the inverse  $\beta$  decay (IBD) is calculated by using the recent analytical results of [16], which take into account

---

\*E-mail: [dnaumov@jinr.ru](mailto:dnaumov@jinr.ru)

\*\*E-mail: [vnaumov@theor.jinr.ru](mailto:vnaumov@theor.jinr.ru)

\*\*\*E-mail: [shkirmanov@theor.jinr.ru](mailto:shkirmanov@theor.jinr.ru)

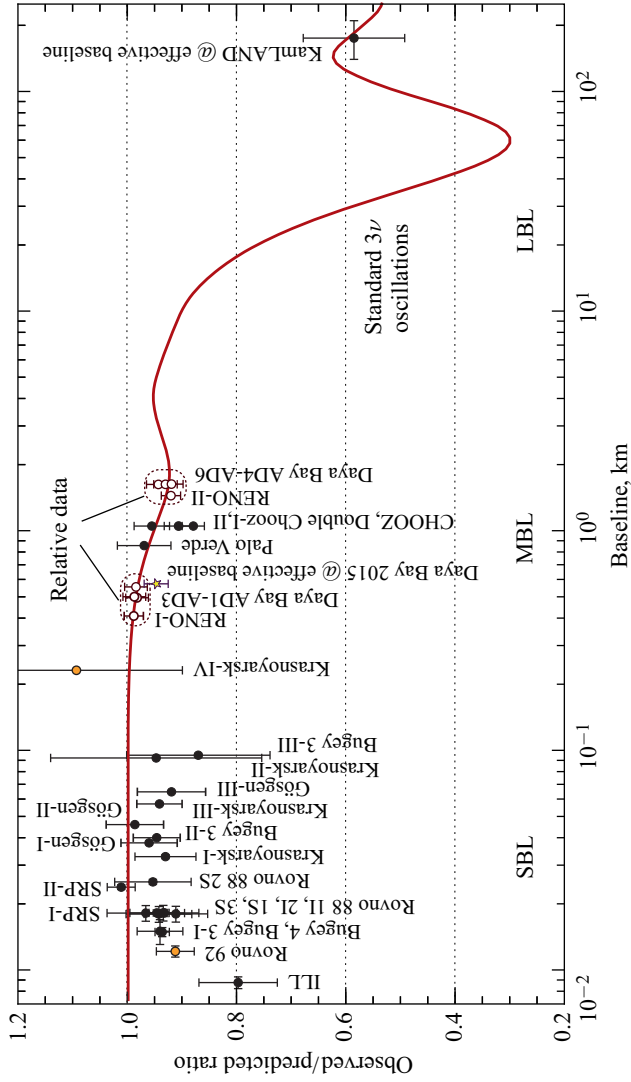


Fig. 1. The reactor antineutrino anomaly. The points represent the ratios of measured event rates to those expected with no oscillations. The vertical error bars do not include the common normalization uncertainty. The original data from [5–14, 17–21] are recalculated as explained in the text. The high-precision data from [22, 23] are relative. The ratios of the KamLAND [21] and Daya Bay 2015 [24] results to the “Huber–Mueller” model predictions are plotted at the flux-weighted distances of 175 km and 573 m, respectively. The curve represents the theoretical expectation, in which the  $3\nu$  oscillations parameters are fixed to the global best fit values taken from the “Review of Particle Physics” [15]; the normal mass ordering and no  $CP$  violation are assumed

the radiative corrections of order  $\alpha/\pi$  and contributions of weak magnetism and neutron recoil to next-to-leading order in the expansion in inverse powers of the nucleon mass. In Fig. 1 and below, all the curves correspond to a reactor with pure  $^{235}\text{U}$  fuel\*. The original data from [5–14, 17–21] are corrected according to [1] and then renormalized to the new world average value of the neutron mean life [15]. It is seen that most of the SBL data points (the measurements at  $L \lesssim 100$  m, where  $L$  is the distance between the reactor core and detector) are below the expectation. A clear trend is visible at  $L \lesssim 20$  m that the closer detector is located to reactor, the smaller the measured rate (the larger the discrepancy between the data and theory). Note that the data points “Krasnoyarsk-IV” [8] and “Rovno 92” [11] are ignored in the numerous RAA analyses, but the latter point is significant for revealing the mentioned trend. Also shown are the data from the medium and long baseline reactor experiments Palo Verde [17], CHOOZ [18], Double Chooz [19,20], KamLAND [21], RENO [22], and Daya Bay [23,24]. The data sets from [22,23] are relative measurements, while the recent high-precision Daya Bay measurement [24] is absolute (in Fig. 1 it is placed at the effective baseline of 573 m). As is seen, the theory is in rather poor agreement with the latter result. Hence, both the earlier SBL and new Daya Bay measurements give a hint to either “new physics” or merely a lower  $\bar{\nu}_e$  flux than predicted in [1,2].

### 1. EXTRA NEUTRINOS OR WRONG NORMALIZATION?

Most if not all efforts to resolve the anomaly are based on the hypothesis of existence of one or more light (eV mass scale) sterile neutrinos, that is, fundamental neutral fermions with no standard model interactions except those induced by mixing with the standard (active) neutrinos. The active-to-sterile neutrino mixing would lead to a distance-dependent spectral distortion and overall reduction of the reactor  $\bar{\nu}_e$  flux.

In Fig. 2 we show, as an example, the results of calculations performed in the framework of the simplest “3 + 1” phenomenological model with one sterile (anti)neutrino,  $\nu_4$ , by using the three pairs of the  $\nu_4 - \nu_1$  mixing parameters,  $(\Delta m_{41}, \sin^2 2\theta_{41})$ , listed in the legend of the figure. These values were derived in [25] from detailed statistical analyses of all the neutrino oscillation data available to date. The “SBL rates only” fit includes the SBL reactor data except the points “Krasnoyarsk-IV” and “Rovno 92” (see Fig. 1). The “SBL + Bugey 3 spectrum” fit includes the same data set and spectral data from Bugey 3 [13]. The “Global  $\nu_e$  disappearance” fit involves the data from the reactor experiments [4, 6–10, 12–14, 17–19, 22, 23, 26], as well as solar neutrinos (261 data points from

---

\*Nevertheless, in the following analysis we explicitly take into account the particular fuel composition in each experiment, since it does have a small impact on the results.

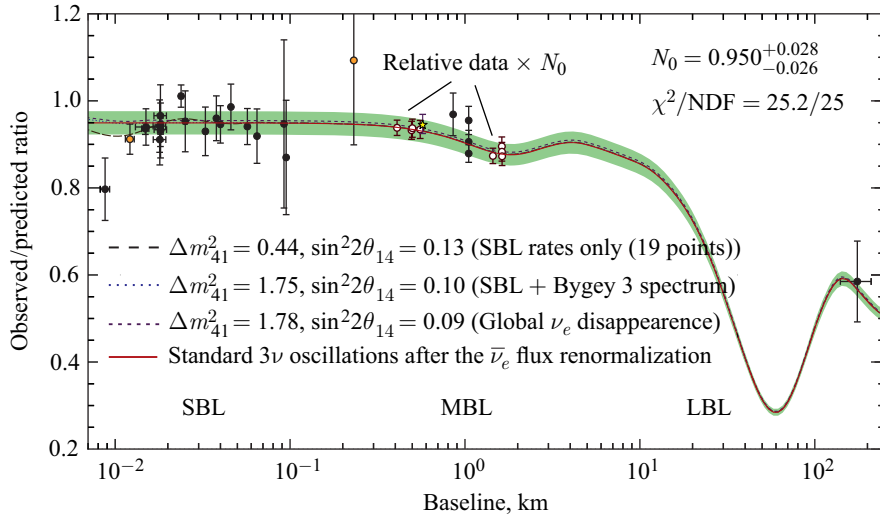


Fig. 2. Comparison of the data with the “3 + 1” model (see text) and with the standard  $3\nu$  oscillation prediction after renormalization of the  $\bar{\nu}_e$  flux (solid curve). The renormalization factor is obtained from a fit to all the data but RENO and Daya Bay. The filled band shows the  $\pm 1\sigma$  uncertainty of the fit. The data points are the same as in Fig. 1 but the eight relative data points (open circles) are shifted by the factor  $N_0 = 0.95$

Homestake, SAGE, GALLEX/GNO, Super-Kamiokande, and SNO experiments), radioactive source experiments at SAGE and GALLEX, and the LSND/KARMEN  $\nu_e$  disappearance data from  $\nu_e - {}^{12}\text{C}$  scattering (see [25] for the full list of references and further details). It is necessary to note that these fits operate with somewhat lower (to within roughly 1%) values for the reactor  $\bar{\nu}_e$  induced rates and with a little bit different covariance matrix, as compared to those used in the present analysis (the details of our calculations will be published elsewhere).

The solid curve in Fig. 2 represents the same  $3\nu$  oscillation prediction as in Fig. 1, but shifted down by the normalization factor  $N_0$  derived from a fit to all the data except these from RENO and Daya Bay. In this fit we take into account the correlation between the data, including the overall normalization uncertainty, which is taken to be 2.7% [3]. The obtained factor  $N_0 = 0.950^{+0.028}_{-0.026}$  ( $\chi^2/\text{NDF} \approx 1$ ) does not contradict the adopted flux uncertainty, but is somewhat different from the results of earlier calculations [3, 16, 27], which used different data subsets and input parameters. All four curves in Fig. 2 are in agreement, within the errors, with the new Daya Bay measurement [24], but are in some conflict with the ILL data point [5].

Recently, it was argued [28] that the true uncertainty in the  $\bar{\nu}_e$  flux predictions may be as large as 5% and the spectral shape uncertainties may be much larger

due to poorly known structure of the forbidden decays. This finding has been in essence confirmed by the new precision measurements of the positron energy spectra from IBD [24], which show apparent  $\sim 10\%$  excess in 4–6 MeV region compared to the expectation based on the models of [1, 2] (see [29] for further discussion and references). From what has been said it appears that the efforts to explain the anomaly by the sterile neutrino hypothesis may be somewhat premature. Moreover, it is seen from Fig. 2 that the proper renormalization of the flux is hardly distinguishable from the “global  $\nu_e$  disappearance”  $4\nu$  fit and (maybe somewhat accidentally) almost fully coincides with the “SBL + Bugey 3 spectrum” fit. We emphasize however that the steady decrease of the event rate at very small  $L$ , *if real*, can be explained by neither the wrong  $\bar{\nu}_e$  flux normalization alone nor the “3 + 1” scenario. Thus, it is appropriate to consider an alternative explanation. Such an alternative has been proposed in [30]. It is based on a quantum field-theoretical (QFT) approach to the neutrino oscillation phenomenon, which in particular predicts a small deviation of the (anti)neutrino event rate, as a function of the distance  $L$  between the source and detector, from the classical inverse-square law (ISL) behavior. Below we consider this issue in some detail.

## 2. A SKETCH OF THE QFT APPROACH

The “neutrino-oscillation” phenomenon in the  $S$ -matrix QFT approach is nothing else than a result of interference of the macroscopic Feynman diagrams (like that shown in Fig. 3) which describe the lepton-number-violating processes with the neutrino mass eigenfields  $\nu_i$  ( $i = 1, 2, 3$ ) treated as internal lines (propagators). The external lines of the macrodiagrams are assumed corresponding to asymptotically free quasi-stable wave packets (WP) rather than the conventional to QFT one-particle Fock’s states  $|\mathbf{k}, s\rangle$  with definite 3-momenta  $\mathbf{k}$  and spin projections  $s$ . According to [31, 32], the free external WP states are constructed as covariant space-time point  $x$  dependent linear superpositions of the one-particle states,

$$|\mathbf{p}, s, x\rangle = \int \frac{d\mathbf{k} \phi(\mathbf{k}, \mathbf{p}) e^{i(k-p)x}}{(2\pi)^3 2E_{\mathbf{k}}} |\mathbf{k}, s\rangle, \quad (1)$$

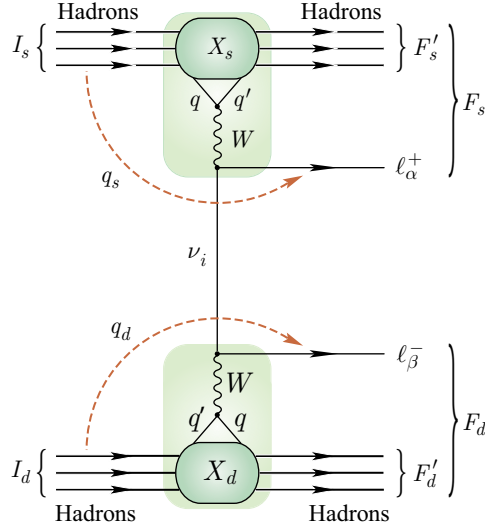
satisfying the *correspondence principle* which demands that  $|\mathbf{p}, s, x\rangle$  turns into  $|\mathbf{k}, s\rangle$  in the plane-wave limit (PWL) that is equivalent to the following condition for the relativistic invariant form factor function  $\phi$ :

$$\phi(\mathbf{k}, \mathbf{p}) \xrightarrow{\text{PWL}} (2\pi)^3 2E_{\mathbf{p}} \delta(\mathbf{k} - \mathbf{p}).$$

The detail properties of the WP states (1) are discussed in [33, 34].

Within the outlined approach, and after applying several more or less “technical” simplifications, it is proved [32] that the neutrino induced event rate in an

Fig. 3. A generic macroscopic Feynman diagram. Here  $I_{s,d}$  and  $F_{s,d}$  denote the sets of the initial ( $I$ ) and final ( $F$ ) WP states in the “source” ( $X_s$ ) and “detector” ( $X_d$ ) vertices;  $F'_{s,d} = F_{s,d} \oplus \ell_{\alpha,\beta}^{\pm}$ , where  $\ell_{\alpha,\beta}^{\pm}$  are the charged lepton WP states ( $\alpha, \beta = e, \mu, \tau$ );  $q_{s,d}$  are the 4-momentum transfers in the vertices, as defined by Eq.(5). The vertices are in general *macroscopically* separated in space and time. The particular “decryption” of the neutrino production/absorption mechanism assumes the standard model charged current interaction of quarks and leptons



ideal detector can be written (somewhat symbolically) in the form

$$\frac{dN}{d\tau} = \frac{1}{V_D V_S} \int_{V_S} d\mathbf{x} \int_{V_D} d\mathbf{y} \int d\tilde{\mathfrak{F}}_\nu \int d\sigma_{\nu\mathcal{D}} \mathcal{P}_{\alpha\beta}(E_\nu, |\mathbf{y} - \mathbf{x}|). \quad (2)$$

Here  $\tau$  is the detector exposure time,  $E_\nu$  is the neutrino energy,  $\mathcal{P}_{\alpha\beta}$  is the QFT generalization of the standard quantum-mechanical neutrino flavor transition probability, the differential form  $d\sigma_{\nu\mathcal{D}}$  represents the differential cross section of the neutrino scattering from the whole detector device;  $d\tilde{\mathfrak{F}}_\nu$  is the differential neutrino flux incident on the detector from a *stationary* source device (e.g., a fission reactor core). The integrations in (2) are over the source and detector fiducial volumes  $V_S$  and  $V_D$ . The theory explicitly predicts that the neutrino flux decreases with increasing the distance  $|\mathbf{y} - \mathbf{x}|$  in compliance with the usual inverse-square law (ISL):

$$d\tilde{\mathfrak{F}}_\nu \propto |\mathbf{y} - \mathbf{x}|^{-2}. \quad (3)$$

This quite expected result has been derived by using the so-called Grimus–Stockinger (GS) theorem [35], which defines the asymptotic behavior of the amplitude at  $L \rightarrow \infty$  and this is the crucial point in the context of the problem under consideration.

As it follows from the formalism, the  $L$  dependence of the amplitude described by the macrodiagram shown in Fig. 3 is defined by the neutrino propagator modified by the external wave packets,

$$(i\hat{\partial} + m_i) \int \frac{d^4 q}{(2\pi)^4} \frac{\tilde{\delta}_s(q - q_s) \tilde{\delta}_d(q + q_d) e^{-iqx}}{q^2 - m_i^2 + i\epsilon}, \quad (4)$$

where  $x = (y_0 - x_0, \mathbf{y} - \mathbf{x}) \equiv (T, \mathbf{L})$ ,  $q_s$  and  $q_d$  are the 4-momentum transfers,

$$q_s = \sum_{a \in I_s} p_a - \sum_{b \in F_s} p_b, \quad q_d = \sum_{a \in I_d} p_a - \sum_{b \in F_d} p_b, \quad (5)$$

$p_{\varkappa}$  are the most probable (on-shell) 4-momenta of the external packets  $\varkappa \in I_s \oplus I_d \oplus F_s \oplus F_d$ , and  $m_i$  is the mass of the neutrino field  $\nu_i$ . The functions  $\tilde{\delta}_s(q - q_s)$  and  $\tilde{\delta}_d(q + q_d)$  are the ‘‘smeared’’  $\delta$  functions (see [30] for their explicit form) defined by the 4-momenta  $p_{\varkappa}$ , masses  $m_{\varkappa}$  ( $m_{\varkappa}^2 = p_{\varkappa}^2$ ), and momentum spreads  $\sigma_{\varkappa}$  of the external in and out packets ( $\sigma_{\varkappa}^2 \lll m_{\varkappa}^2$ ). In the plane-wave limit ( $\sigma_{\varkappa} \rightarrow 0, \forall \varkappa$ ) these functions turn into the ordinary Dirac  $\delta$  functions,  $\tilde{\delta}_s(q - q_s) \xrightarrow{\text{PWL}} \delta(q - q_s), \tilde{\delta}_d(q + q_d) \xrightarrow{\text{PWL}} \delta(q + q_d)$ , thus leading to the exact energy-momentum conservation in the vertices of the macrodiagram, and the function (4) becomes, up to a multiplier, the standard fermion propagator. If, however, the momentum spreads  $\sigma_{\varkappa}$  are finite, the space-time behavior of the function (4) is nontrivial. In particular, its spatial dependence at sufficiently large distances  $L$  is given by the above-mentioned GS theorem [35], according to which\*

$$J(\mathbf{L}, \kappa) = \int \frac{d\mathbf{q}}{(2\pi)^3} \frac{\Phi(\mathbf{q}) e^{i\mathbf{q}\mathbf{L}}}{\mathbf{q}^2 - \kappa^2 - i\epsilon} = \frac{e^{i\kappa L} \Phi(-\kappa\mathbf{1})}{4\pi L} \left[ 1 + \mathcal{O}\left(\frac{\infty}{\sqrt{\mathcal{L}}}\right) \right] \quad \left( \mathbf{1} = \frac{\mathbf{L}}{L} \right)$$

as  $L = |\mathbf{L}| \rightarrow \infty$ . This offers the QFT explanation of the ISL behavior (3) but does not, however, provide the spatial scale above which the distance  $L$  may be considered as ‘‘sufficiently large’’.

In [30], an extended version of the GS theorem has been proved, which parametrically defines such a scale by using the asymptotic expansion of the integral  $J(\mathbf{L}, \kappa)$  in terms of inverse powers of  $L$  at large  $L$ . To be more precise, the theorem in its simplest form states that for any function  $\Phi(\mathbf{q})$  in the Schwartz space  $S(\mathbb{R}^3)$

$$J(\mathbf{L}, \kappa) = \frac{e^{i\kappa L}}{4\pi L} \left[ \Phi(\mathbf{q}) + \sum_{n \geq 1} \frac{(-i)^n D_n \Phi(\mathbf{q})}{L^n} \right]_{\mathbf{q} = -\kappa\mathbf{1}}, \quad L \rightarrow \infty, \quad (6)$$

where  $D_n$  are explicitly defined differential operators on the momentum space; the lowest order operators, sufficient for our present purpose, are

$$D_1 = \frac{\kappa}{2} [\nabla_{\mathbf{q}}^2 - (\mathbf{1}\nabla_{\mathbf{q}})^2] - (\mathbf{1}\nabla_{\mathbf{q}}),$$

$$D_2 = \frac{\kappa^2}{8} [\nabla_{\mathbf{q}}^2 - (\mathbf{1}\nabla_{\mathbf{q}})^2]^2 - \kappa(\mathbf{1}\nabla_{\mathbf{q}})[\nabla_{\mathbf{q}}^2 - (\mathbf{1}\nabla_{\mathbf{q}})^2] - \frac{1}{2} [\nabla_{\mathbf{q}}^2 - 3(\mathbf{1}\nabla_{\mathbf{q}})^2].$$

---

\*It is assumed that the complex-valued function  $\Phi(\mathbf{q})$  itself and its first and second derivatives decrease at least like  $1/|\mathbf{q}|^2$  as  $|\mathbf{q}| \rightarrow \infty$  and  $\kappa^2 > 0$ ; see [30] for details.

Additional important features can be found in [30, 36]. An analysis of Eq. (6) shows that the  $1/L$  behavior of the amplitude (and thus the ISL behavior of the event rate) is violated at the distances  $L \lesssim \mathcal{L}_0$ , where

$$\mathcal{L}_0 \sim \kappa \sigma_{\text{eff}}^{-2} \approx 20 \left( \frac{\kappa}{1 \text{ MeV}} \right) \left( \frac{\sigma_{\text{eff}}}{1 \text{ eV}} \right)^{-2} \text{ cm} \tag{7}$$

and the function  $\sigma_{\text{eff}} = \sigma_{\text{eff}}(\kappa; \{\mathbf{v}_\varkappa, m_\varkappa, \sigma_\varkappa\})$  represents an effective momentum spread dependent on the neutrino momentum  $\kappa$  as well as on the mean velocities, masses, and momentum spreads of the external (in and out) wave packets  $\varkappa$ . The explicit form of this function can be found after specification of a particular model for the external WP states. A simple example is discussed in [30] within the so-called contracted relativistic Gaussian packet (CRGP) model [33, 34]. It is in particular shown that  $\sigma_{\text{eff}}$  is defined through the transverse (with respect to the neutrino propagation direction  $\mathbf{l}$ ) components of the inverse overlap tensors which determine the effective space-time overlap volumes of the WP states in the vertices of the macrodiagram. It is significant that these components are nearly independent of the neutrino masses (assuming these to be small with respect to the neutrino energy and thus  $\kappa \simeq E_\nu$ ). Within the CRGP model, it can also be shown that the magnitude of  $\sigma_{\text{eff}}$  is strongly affected by the hierarchy of the external momentum spreads  $\sigma_\varkappa$  but in the simplest case when these spreads are similar in order of magnitude,  $\sigma_{\text{eff}}$  is of the same order, too. So, as is seen from Eq. (7), the spatial scale (7) can be macroscopically large at sufficiently small external momentum spreads, thus leading to a measurable ISL violation (ISLV).

It is shown in [33] that Eq. (6) modifies the formula for the event rate (2) in such a way that the relation (3) for the flux is replaced by

$$d\mathfrak{F}_\nu \propto \frac{1}{|\mathbf{y} - \mathbf{x}|^2} \left( 1 + \sum_{n \geq 1} \frac{\mathfrak{C}_n}{|\mathbf{y} - \mathbf{x}|^{2n}} \right), \tag{8}$$

where the coefficient functions  $\mathfrak{C}_n$  are explicitly defined from Eq. (6). By making expedient assumptions, it can be proved (and this is a crucial point) that  $\mathfrak{C}_1 < 0$ . Hence, using Eq. (8) in leading order (thereby assuming that the ISLV correction is small) yields the following simple replacement for the event rate:

$$\frac{dN}{d\tau} \mapsto \left( 1 - \frac{\overline{\mathfrak{T}}_0^2}{L^2} \right) \frac{dN}{d\tau} \tag{9}$$

(provided that  $\overline{\mathfrak{T}}_0^2 \ll L^2$ ). Here  $\overline{\mathfrak{T}}_0 \sim \langle \mathcal{L}_0 \rangle$  is a neutrino energy dependent parameter of dimension of length. Needless to say, at present this parameter cannot be obtained from first-principle calculations, but it can be measured.

### 3. DATA ANALYSIS

To check the assumption that the ISLV effect could actually be, in part, responsible for RAA, we performed a statistical analysis of the reactor data discussed in Introduction. Since in this paper we use only the spectrum-averaged event rates, the  $L$  dependent factor in Eq. (9) can be replaced by  $(1 - L_0^2/L^2)$ , where  $L_0 \sim \langle \bar{L}_0 \rangle$  is an energy independent parameter, which is a subject of the present study. Taking into account the large uncertainty in the  $\bar{\nu}_e$  flux normalization, we shall use the following theoretical model to fit the data:

$$T(L; N_0, L_0) = N_0 \left(1 - \frac{L_0^2}{L^2}\right) \frac{\int_0^\infty dE_\nu \sum_k f_k P_{\text{surv}}^{3\nu}(L, E_\nu) \sigma(E_\nu) S_k(E_\nu)}{\int_0^\infty dE_\nu \sum_k f_k \sigma(E_\nu) S_k(E_\nu)}. \quad (10)$$

Here  $N_0$  is the required normalization parameter,  $f_k$  is the reactor fissile isotope fraction,  $S_k(E_\nu)$  is the  $\bar{\nu}_e$  energy spectrum (taken from [1]),  $\sigma(E_\nu)$  is the IBD cross section [16] and  $P_{\text{surv}}^{3\nu}(L, E_\nu)$  is the  $\bar{\nu}_e$  survival probability in the standard  $3\nu$  mixing scheme\*. In order to find the best-fit parameters  $N_0$  and  $L_0$ , we minimize the standard  $\chi^2$  with the full covariance matrix for the correlated data. The results of the fits of several types are shown in Figs. 4–6.

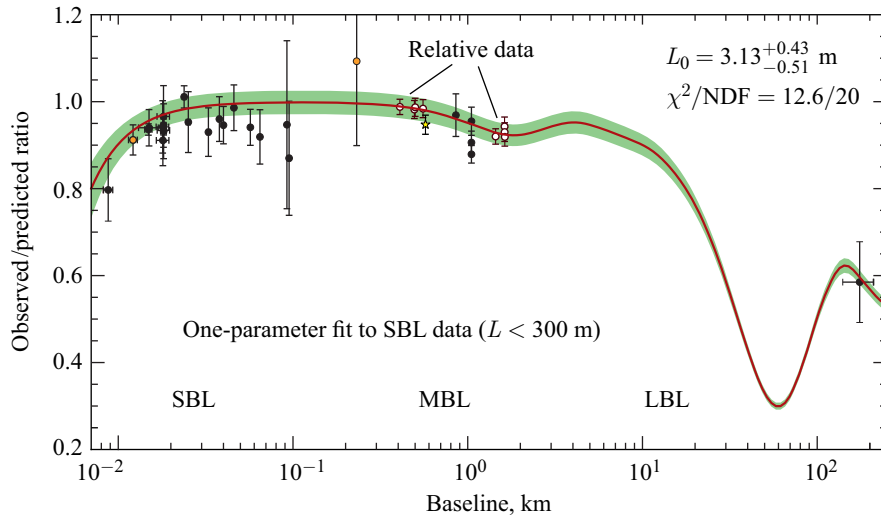


Fig. 4. One-parameter fit to the SBL data set assuming  $N_0 = 1$

\*We thereby neglect the decoherence effects predicted in the QFT approach [32], reasonably assuming that the baselines under consideration are too short for their manifestation.

Figure 4 represents the results of the simplest one-parameter fit, in which  $N_0$  is set to 1 and only the SBL data ( $L < 300$  m) are used in the analysis. Here and below, the filled band represents the  $\pm 1\sigma$  uncertainty. It is seen that despite relatively small value of  $\chi^2/\text{NDF}$  the best-fit curve is in rather poor agreement with the data; in particular, it is in conflict with the recent Daya Bay

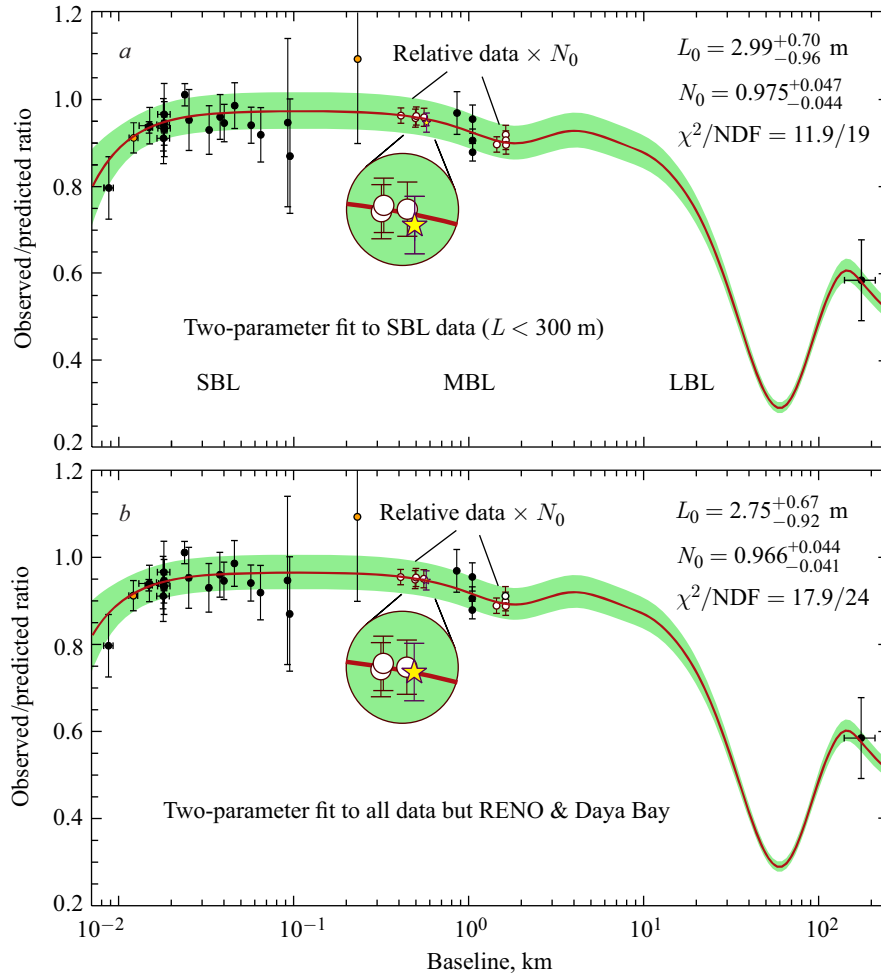


Fig. 5. Two-parameter fits to the SBL data subset (a) and to the full (SBL + MBL + LBL) reactor data set (b); the data of RENO [22] and Daya Bay [23,24] are not included into the statistical analysis. The eight relative data points in the panels a and b are shifted by the factors 0.975 and 0.966, respectively. The inserts clarify the agreement between the best-fit curves and Daya Bay relative and absolute data points

measurement. This indicates that the ISLV suppression alone is not sufficient and the flux renormalization is actually required.

Figure 5 illustrates the results of the two-parameter fits performed with two different data subsets, namely with the SBL data only, and with all the data except those from RENO and Daya Bay. As is seen from the figure, these two fits are in reasonable agreement with each other and both describe the reactor data rather well. Although the value of  $\chi^2/\text{NDF}$  for the SBL data is nominally a bit better than that for the fit to all data (0.63 and 0.74, respectively), the latter fit is (as is clearly seen in the inserts of Fig. 5) in better agreement with the Daya Bay point (let us remind that it does not participate in the analysis). By comparing these results with the fits shown in Fig. 2, we may conclude that the ISLV effect in combination with the proper renormalization of the  $\bar{\nu}_e$  flux provides a better resolution of the anomaly.

To gain a bit deeper understanding of our results, we compare in Fig. 6 the 68% C.L. error contours for the pair of the fitted parameters  $(N_0, L_0)$ , obtained from the fits to different data subsets. Figure 6, *a* shows the contours for the fits to all data and SBL data subset. Figure 6, *b* shows the same but with the ILL data point excluded from the analysis. It is seen with no need of additional explanation that the Grenoble experiment is the “cornerstone” for verification of the ISLV effect. It is, however, quite remarkable that even without the ILL point we obtain essentially the same best-fit values for the parameters  $N_0$  and  $L_0$ .

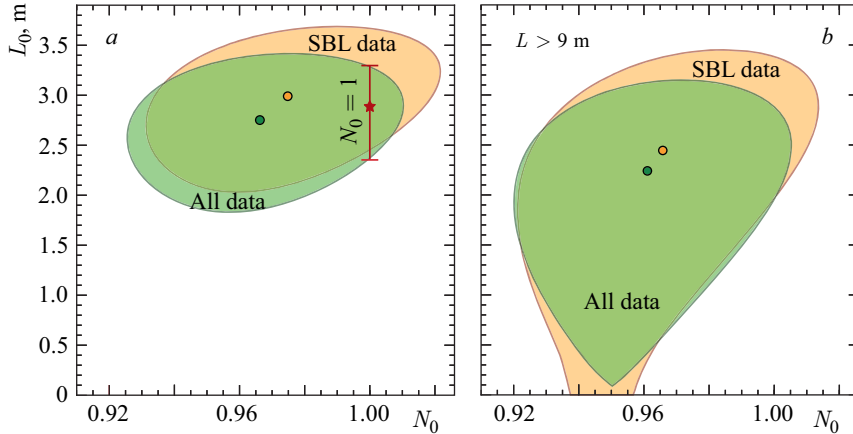


Fig. 6. *a*) The 68% C.L. error contours for the pair of the parameters  $N_0$  and  $L_0$  extracted from the fits to all data and SBL data subset ( $L < 300$  m). The one-parameter (with  $N_0$  fixed to 1) fit to SBL data is also shown for comparison. *b*) The same as in panel *a*, but with the ILL data point excluded from the statistical analysis. In both panels, the circles correspond to the best-fit values of the parameters  $(N_0, L_0)$  with  $L_0^{\text{SBL data}} > L_0^{\text{All data}}$  and  $N_0^{\text{SBL data}} > N_0^{\text{All data}}$ .

## CONCLUSIONS

The QFT approach predicts a deviation from the classical inverse-square law at short baselines. While the numerical value of the spatial scale at which the deviation becomes essential cannot be predicted from the present-day theory, it can be extracted, under reasonable assumptions, from the data of the past and current reactor antineutrino experiments. Our statistical analysis demonstrates that the value of the scale ( $L_0$ ) averaged over the reactor antineutrino spectrum is about 3 m, which roughly corresponds to the spectrum-averaged effective momentum spread  $\langle\sigma_{\text{eff}}\rangle$  of about 0.5–0.8 eV (thereby hinting that the wave packets of the particles and nuclei involved in the reactor  $\bar{\nu}_e$  production and detection may have “mesoscopic” effective dimensions). This is in agreement with the conservative estimate presented in [30]. Besides, the best-fit value of  $L_0$  is very stable with respect to choice of the data subset and  $\bar{\nu}_e$  spectrum model. To check the latter, we performed the same one- and two-parameter fits as described above, but with the input  $\bar{\nu}_e$  energy spectra from [37] and [38] derived by very different methods, as well as with combinations of the models [1,2] and the cumulative  $\bar{\nu}_e$  spectrum from  $^{238}\text{U}$  fission recently measured with the scientific neutron source FRM II in Garching [39]. We conclude from these exercises that value of  $L_0$  is almost insensitive (within the errors) to the spectrum variations. Needless to say, it is not the case for the normalization parameter  $N_0$ .

Although the available reactor data cannot definitely confirm or exclude the light sterile neutrino hypothesis, and do not provide unambiguous support for the ISLV effect, they are in much better agreement with the latter. The next-generation experiments with very short baselines ( $L \lesssim 20$  m), small neutrino or antineutrino sources, and high-precision, desirably movable detectors are required in order to confirm or disconfirm our explanation.

## REFERENCES

1. *Mueller Th. A. et al.* Improved Predictions of Reactor Antineutrino Spectra // Phys. Rev. C. 2011. V. 83. P. 054615.
2. *Huber P.* On the Determination of Antineutrino Spectra from Nuclear Reactors // Phys. Rev. C. 2011. V. 84. P. 024617; Erratum // Phys. Rev. C. 2012. V. 85. P. 029901.
3. *Mention G. et al.* The Reactor Antineutrino Anomaly // Phys. Rev. D. 2011. V. 83. P. 073006.
4. *Kwon H. et al.* Search for Neutrino Oscillations at a Fission Reactor // Phys. Rev. D. 1981. V. 24. P. 1097–1111.
5. *Hoummada A. et al.* Neutrino Oscillations I.L.L. Experiment Reanalysis // Appl. Rad. Isot. 1995. V. 46. P. 449–450.

6. *Zacek G. et al.* Neutrino Oscillation Experiments at the Gösigen Nuclear Power Reactor // *Phys. Rev. D.* 1986. V. 34. P. 2621–2636.
7. *Vidyakin G. S. et al.* Detection of Antineutrinos in the Flux from Two Reactors // *Zh. Eksp. Teor. Fiz.* 1987. V. 93. P. 434–421.
8. *Vidyakin G. S. et al.* Limitations on the Characteristics of Neutrino Oscillations // *Pisma Zh. Eksp. Teor. Fiz.* 1994. V. 59. P. 364–367.
9. *Afonin A. I. et al.* A Study of the Reaction  $\tilde{\nu}_e + p \rightarrow e^+n$  on a Nuclear Reactor // *Zh. Eksp. Teor. Fiz.* 1988. V. 94. P. 1–17.
10. *Kuvshinnikov A. A. et al.* Precise Measurement of the Cross Section for the Reaction  $\tilde{\nu}_e + p \rightarrow e^+n$  at a Reactor of the Rovno Nuclear Power Plant // *Pisma Zh. Eksp. Teor. Fiz.* 1991. V. 54. P. 259–262.
11. *Ketov S. N. et al.* Reactor Experiments of a New Type to Detect Neutrino Oscillations // *Pisma Zh. Eksp. Teor. Fiz.* 1992. V. 55. P. 544–547.
12. *Declais Y. et al.* Study of Reactor Antineutrino Interaction with Proton at Bugey Nuclear Power Plant // *Phys. Lett. B.* 1994. V. 338. P. 383–389.
13. *Achkar B. et al.* Search for Neutrino Oscillations at 15, 40 and 95 Meters from a Nuclear Power Reactor at Bugey // *Nucl. Phys. B.* 1995. V. 434. P. 503–534.
14. *Greenwood Z. D. et al.* Results of a Two Position Reactor Neutrino Oscillation Experiment // *Phys. Rev. D.* 1996. V. 53. P. 6054–6064.
15. *Olive K. A. et al. (Particle Data Group Collab.).* Review of Particle Physics // *Chin. Phys. C.* 2014. V. 38. P. 090001.
16. *Ivanov A. N. et al.* Deficit of Reactor Antineutrinos at Distances Smaller Than 100 m and Inverse  $\beta$ -Decay // *Phys. Rev. C.* 2013. V. 88. P. 055501.
17. *Boehm F. et al.* Final Results from the Palo Verde Neutrino Oscillation Experiment // *Phys. Rev. D.* 2001. V. 64. P. 112001.
18. *Apollonio M. et al. (CHOOZ Collab.).* Search for Neutrino Oscillations on a Long Baseline at the CHOOZ Nuclear Power Station // *Eur. Phys. J. C.* 2003. V. 27. P. 331–374.
19. *Abe Y. et al. (Double Chooz Collab.).* Reactor Electron Antineutrino Disappearance in the Double Chooz Experiment // *Phys. Rev. D.* 2012. V. 86. P. 052008.
20. *Abe Y. et al. (Double Chooz Collab.).* First Measurement of  $\theta_{13}$  from Delayed Neutron Capture on Hydrogen in the Double Chooz Experiment // *Phys. Lett. B.* 2013. V. 723. P. 66–70.
21. *Araki T. et al. (KamLAND Collab.).* Measurement of Neutrino Oscillation with KamLAND: Evidence of Spectral Distortion // *Phys. Rev. Lett.* 2005. V. 94. P. 081801.
22. *Ahn J. K. et al. (RENO Collab.).* Observation of Reactor Electron Antineutrino Disappearance in the RENO Experiment // *Phys. Rev. Lett.* 2012. V. 108. P. 191802.
23. *An F. P. et al. (Daya Bay Collab.).* Improved Measurement of Electron Antineutrino Disappearance at Daya Bay // *Chin. Phys. C.* 2013. V. 37. P. 011001.

24. *Naumov D. V.* Recent Results from Daya Bay Experiment // EPJ Web Conf. 2015. V. 95. P. 04043.
25. *Kopp J. et al.* Sterile Neutrino Oscillations: The Global Picture // JHEP. 2013. V. 05. P. 050.
26. *Gando A. et al. (KamLAND Collab.)*. Constraints on  $\theta_{13}$  from a Three-Flavor Oscillation Analysis of Reactor Antineutrinos at KamLAND // Phys. Rev. D. 2011. V. 83. P. 052002.
27. *Zhang C., Qian X., Vogel P.* Reactor Antineutrino Anomaly with Known  $\theta_{13}$  // Phys. Rev. D. 2013. V. 87. P. 073018.
28. *Hayes A. C. et al.* Systematic Uncertainties in the Analysis of the Reactor Neutrino Anomaly // Phys. Rev. Lett. 2014. V. 112. P. 202501.
29. *Dwyer D. A., Langford T. J.* Spectral Structure of Electron Antineutrinos from Nuclear Reactors // Phys. Rev. Lett. 2015. V. 114. P. 012502.
30. *Naumov V. A., Shkirmanov D. S.* Extended Grimus–Stockinger Theorem and Inverse Square Law Violation in Quantum Field Theory // Eur. Phys. J. C. 2013. V. 73. P. 2627.
31. *Naumov V. A., Naumov D. V.* Relativistic Wave Packets in a Field Theoretical Approach to Neutrino Oscillations // Russ. Phys. J. 2010. V. 53. P. 549–574.
32. *Naumov D. V., Naumov V. A.* A Diagrammatic Treatment of Neutrino Oscillations // J. Phys. G. 2010. V. 37. P. 105014.
33. *Naumov D. V.* On the Theory of Wave Packets // Phys. Part. Nucl. Lett. 2013. V. 10, No. 7. P. 642–650.
34. *Naumov V. A., Shkirmanov D. S.* Covariant Asymmetric Wave Packet for a Field-Theoretical Description of Neutrino Oscillations // Mod. Phys. Lett. A. 2015. V. 30. P. 1550110.
35. *Grimus W., Stockinger P.* Real Oscillations of Virtual Neutrinos // Phys. Rev. D. 1996. V. 54. P. 3414–3419.
36. *Korenblit S. E., Taychenachev D. V.* Extension of Grimus–Stockinger Formula from Operator Expansion of Free Green Function // Mod. Phys. Lett. A. 2015. V. 30. P. 1550074.
37. *Fallot M. et al.* New Antineutrino Energy Spectra Predictions from the Summation of Beta Decay Branches of the Fission Products // Phys. Rev. Lett. 2012. V. 109. P. 202504.
38. *Sinev V. V.* Experimental Spectrum of Reactor Antineutrinos and Spectra of Main Fissile Isotopes // Yad. Fiz. 2013. V. 76. P. 578–584.
39. *Haag N. et al.* Experimental Determination of the Antineutrino Spectrum of the Fission Products of  $^{238}\text{U}$  // Phys. Rev. Lett. 2014. V. 112. P. 122501.